Surface Science 652 (2016) 286–293

Contents lists available at ScienceDirect

Surface Science

journal homepage: www.elsevier.com/locate/susc

Exploring Pd adsorption, diffusion, permeation, and nucleation on bilayer SiO_2/Ru as a function of hydroxylation and precursor environment: From UHV to catalyst preparation

Sascha Pomp [a,b], William E. Kaden [a,*,1], Martin Sterrer [a,b,*], Hans-Joachim Freund [a]

[a] Department of Chemical Physics, Fritz Haber Institute of the Max Planck Society, Faradayweg 4-6, D-14195, Berlin, Germany
[b] Institute of Physics, University of Graz, Universitätsplatz 5, A-8010 Graz, Austria

ARTICLE INFO

Available online 6 January 2016

Keywords:
Model catalyst
Palladium
Silica
Thin film
Hydroxylation
Catalyst preparation

ABSTRACT

The hydroxylation-dependent permeability of bilayer SiO_2 supported on Ru(0001) was investigated by XPS and TDS studies in a temperature range of 100 K to 600 K. For this, the thermal behavior of Pd evaporated at 100 K, which results in surface and sub-surface (Ru-supported) binding arrangements, was examined relative to the extent of pre-hydroxylation. Samples containing only defect-mediated hydroxyls showed no effect on Pd diffusion through the film at low temperature. If, instead, the concentration of strongly bound hydroxyl groups and associated weakly bound water molecules was enriched by an electron-assisted hydroxylation procedure, the probability for Pd diffusion through the film is decreased via a pore-blocking mechanism. Above room temperature, all samples showed similar behavior, reflective of particle nucleation above the film and eventual agglomeration with any metal atoms initially binding beneath the film. When depositing Pd onto the same SiO_2/Ru model support via adsorption of $[Pd(NH_3)_4]Cl_2$ from alkaline (pH 12) precursor solution, we observe notably different adsorption and nucleation mechanisms. The resultant Pd adsorption complexes follow established decomposition pathways to produce model catalyst systems compatible with those created exclusively within UHV despite lacking the ability to penetrate the film due to the increased size of the initial Pd precursor groups.

1. Introduction

Due to the versatile application of silicates across many fields, such as geology, microelectronics, energy conversion, and catalysis, bettering the fundamental understanding of such materials remains of great interest to the scientific community at large [1]. Recent developments allowing for the growth and detailed characterization of ultrathin silica films over various metal supports have opened new pathways to such information, as illustrated by several publications over the past decade [2–8].

Of the many films developed, the two that stand out as the most widely studied variants are monolayer $SiO_{2.5}$/Mo(112) and bilayer SiO_2/Ru(0001) [2,6]. In both cases, the film consists of corner-sharing SiO_4 tetrahedra moieties joined together to create ordered, 6-membered, lateral honeycomb arrays with similar unit cell dimensions. While the thinner film self-terminates at a single monolayer due to strong Si-O-Mo bonds, the Ru-supported film has been shown to adapt a decoupled and fully saturated bilayer structure, which may exist in either crystalline or vitreous phases with respect to the surface plane. For the latter, these phases typically coexist to varying degrees as separate domains within the bilayer films depending on the specific preparation conditions employed [9–11]. In the case of the vitreous domains, the presence of differently sized pores leads to the creation of membranes capable of selectively passing or blocking the diffusion of various atoms and molecules through the film depending on the presence or absence of silica rings larger than various permeation thresholds, as has been shown for various gases, like CO and D_2 [12], and metal atoms, like Pd and Au [13,14].

While the development of silica films capable of acting like size, atomic, and/or molecular sieves has clear utilizations in a number of potential applications, the ability to reversibly tailor this characteristic in situ and better understand how it changes under various conditions are both likely to be of critical importance when optimizing the effect under varying environments when used in more applied settings. As shown previously, an ability to alternate between the crystalline and vitreous phases of the film could provide a means of tailoring its permeability towards various adsorbates [13], but this has unfortunately proven difficult to reliably control in practice and necessitates sample temperatures far above those practical for many potential applications before bond rearrangement within the film becomes notable (≈1200 K). By contrast, chemically controlled manipulation of surface termination, such as the creation or removal of hydroxyl groups,

* Corresponding authors.
E-mail addresses: william.kaden@ucf.edu (W.E. Kaden), martin.sterrer@uni-graz.at (M. Sterrer).
[1] Present address: Department of Physics, University of Central Florida, 4111 Libra Drive, Physical Sciences Building 308, Orlando, FL 32816, USA.

http://dx.doi.org/10.1016/j.susc.2015.12.030
0039-6028/

which have been shown to act as anchor sites for various metal species diffusing over other oxide supports [15,16], may provide a better means of tailoring diffusion processes on and through the film under a wider range of conditions. While results from previous work demonstrated only limited hydroxyl formation at native defect sites following preparation and exposure to water vapor at low temperature [17], more recent research has provided a means of significantly increasing the number of hydroxyl groups created following a similar procedure in tandem with electron bombardment, which will be the main focus of a forthcoming publication [18]. Following this approach, we have explored the impact of hydroxyl groups in governing the adsorption, diffusion, and nucleation of Pd on and through the porous bilayer SiO_2 membrane under a variety of conditions within ultrahigh vacuum (UHV) and used the insights garnered from the conventional surface-science experiments to better understand the dynamics at play when producing model systems under more industrially relevant conditions, such as adsorption of Pd onto silica from aqueous precursor solution.

2. Experimental details

The experiments conducted for the present study were performed within a UHV chamber (base pressure 3×10^{-10} mbar) equipped with low energy electron diffraction (LEED; Specs, ErLEED), temperature-programmed desorption (TPD; Pfeiffer Vacuum, QMG 220), and X-ray photoemission spectroscopy (XPS, Al Kα; Specs, XR50 Source and PHOIBOS 150 Detector). Sample temperature was measured using a K-type thermocouple that was spot-welded directly to the edge of the ruthenium crystal, which was controllably heated and cooled within a range from ~100–1500 K using a liquid nitrogen cooling reservoir housed within the sample manipulator and an electron bombardment filament positioned directly behind the crystal.

In all cases, bilayer sheets of silica were produced over the Ru(0001) single-crystal, which was first cleaned by several cycles of Ar^+-sputtering and UHV annealing using film growth parameters equivalent to those described elsewhere [11]. Briefly, the protocol consisted of evaporating ~1.6×10^{15} atoms/cm^2 Si onto preoxidized, 3O-(2×2)/Ru(0001) at $T \leq 150$ K, and then annealing at $T \approx 1200$ K in the presence of 2×10^{-6} mbar O_2 before cooling the sample to ~600 K within the same environment prior to restoring vacuum to allow for subsequent manipulation and experimentation. As both cooling rate and Si coverage have been suggested to potentially impact the overall film quality, we employed the same cooling rate (~1 K/s) and relative Si concentrations (±5% via XPS analysis) in all preparations, which results in films exhibiting a mixture of both amorphous and crystalline phases within the 2D bilayer [8]. For brevity, such films will be referred to as SiO_2/Ru throughout the remainder of this paper.

Post film growth, both LEED and XPS characterization were employed in a manner consistent with that described elsewhere to ensure sample compatibility throughout the study [11]. Once created and characterized, the films were either used as is or exposed to 5 L D_2O at 100 K. For experiments aimed at producing larger hydroxyl coverages, the ice-covered samples were subsequently irradiated with a flux of high-energy electrons (50 μA at 200 V) for 60 s. Within UHV, exposure to water was accomplished using a directional dosing tube positioned directly in front of the sample to reduce the residual exposure to the chamber, and the electron beam was generated using a thoriated tungsten filament positioned ~2 cm from the sample surface. Notably, no peaks indicative of adventitious contamination were detectable by XPS following electron bombardment. For TPD measurements, the sample was positioned directly in front of the skimmer cone, encapsulating the differentially pumped mass spectrometer and heated at a rate of 9 K/s. Within UHV, Pd was deposited over the various samples at ~100 K using an electron beam evaporator (Omicron, EFM3T), and fluxes were established with the aid of quartz micro-balance (Inficon, SQM-160) calibration, with resultant surface concentrations verified via XPS. It is noteworthy to point out that the XPS data reported herein show a systematic increase of ~0.35 eV relative to previously reported results due to a recent recalibration of the electronics governing the hemispherical analyzer, such that the $3d_{5/2}$ binding energy (BE) measured from Pd(111) has shifted from a previous value of 335.05 eV to the current value of 335.4 eV. For simplicity, all subsequent discussions of Pd XPS will also focus on changes to the 5/2 components of the 3d doublet, as the relative effects on the corresponding 3/2 components are identical but separated from the larger peak by a fixed ΔBE shift of +5.26 eV.

Liquid-phase experiments were conducted by removing the air-stable SiO_2/Ru samples from UHV through an argon-filled transfer-chamber and then exposing only the sample surface to aqueous environments within a hanging meniscus configuration. The deposition of Pd was accomplished by exposing the sample to 1000 ppm $[Pd(NH_3)_4]Cl_2$ for 1 h within an aqueous solution of pH 12 NaOH, which was chosen to be consistent with recipes reported elsewhere for the production of Pd/SiO_2 catalytic materials [19–24]. Following liquid exposure, samples were blown dry in a flow of helium before reintroduction to the UHV system following placement within and subsequent evacuation of the transfer-chamber.

3. Results and discussion

3.1. Coverage effects and thermal stability of Pd on SiO_2/Ru

As an extension of previous work dedicated to the characterization of small concentrations of Pd deposited on SiO_2/Ru at low temperature [13,25], we conducted a series of temperature-dependent XPS

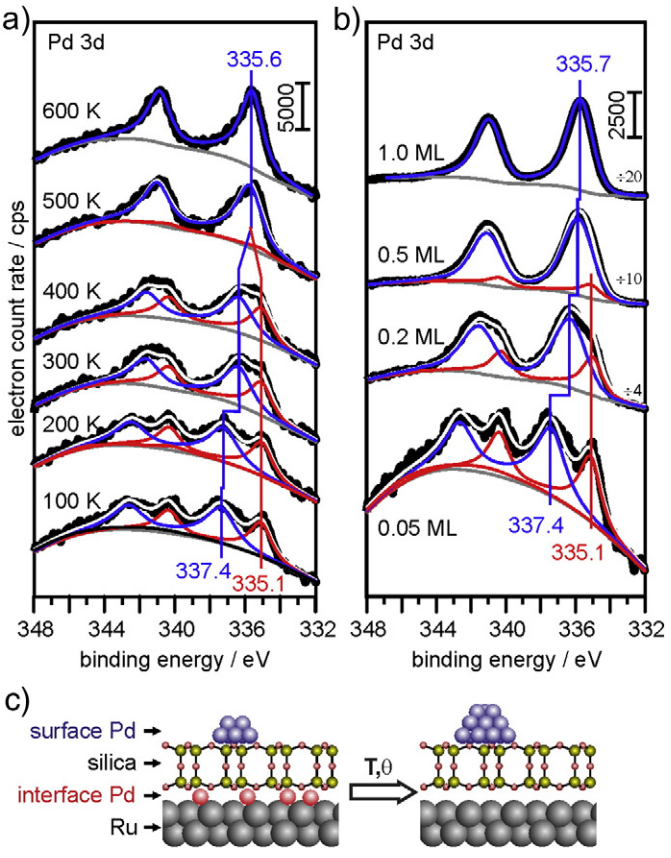

Fig. 1. (a) Pd 3d XPS spectra are provided for SiO_2/Ru samples covered with 0.05 ML Pd at 100 K and sequentially heated to 600 K in 100 K increments. (b) Pd 3d XPS spectra are provided for SiO_2/Ru samples exposed to increasing coverages (0.05, 0.20, 0.50, and 1.00 ML) of Pd at 100 K. (c) Schematic showing the interface and surface binding configurations of low coverage Pd on bilayer silica (left) and the effect of increasing coverage and temperature (right).

measurements consistent with that shown in Fig. 1a for Pd coverages of 0.05 (shown), 0.2, 0.5, and 1 ML (1 ML = 1.53×10^{15} Pd/cm^2) deposited at 100 K. Consistent with previous results, two clearly resolved features appear when probing Pd 3d XPS following exposure to the smallest concentration at 100 K (bottom trace), which have been attributed to atoms that either nucleated to form small clusters on the SiO_2 film (broader feature at 337.4 eV) or diffused through the pores of the film to bind at the underlying Ru interface (sharper feature at 335.1 eV), see schematic shown in Fig. 1c. Note that the curved background is attributed to a broad Ru feature present in the absence of Pd, and that this has been accounted for via comparison with uncovered SiO_2/Ru samples. As more Pd is deposited over the film (Fig. 1b), the likelihood of surface nucleation becomes increasingly probable, such that the relative abundance of silica-bound Pd grows steadily relative to that diffusing through the film, and this coincides with a growth in the average size of those clusters [13]. These trends are reflected in Fig. 1b as a continual growth of the higher BE feature relative to its lower BE counterpart and a gradual shift of that feature to lower BE with smaller peak widths as Pd exposure increases, such that the contribution from Ru-bound Pd becomes essentially negligible and the peak location of the SiO_2-bound Pd becomes more consistent with bulk metal at higher loadings [13].

Interestingly, heating Pd-covered samples results in trends similar to those observed when increasing loading at low temperature. For the most extreme case (0.05 ML), we see little change in the Pd 3d spectrum upon heating to 200 K, indicating that the Pd structures formed following exposure at 100 K remain stable throughout that temperature range. By contrast, we note downward BE shifts associated with the silica-bound particles above 300 K, which reflects mobilization of Pd in this temperature range to result in progressively larger supported clusters [13,26,27]. As this trend continues at higher temperatures, the Pd eventually ends up in a state virtually equivalent to that formed when exposing the sample to 1 ML at 100 K, such that the two components are no longer distinguishable and produce a single $3d_{5/2}$ XPS feature centered at ~335.6 eV. Notably, the peak convergence appears to result at least partially from the disappearance of the lower BE feature, which suggests that the silica-bound cluster growth includes some degree of interaction with Ru-bound atoms to increase their measured BEs (i.e., particle agglomeration includes some degree of diffusion into or out of the silica pores to either tether the supported clusters to the underlying metal or decouple those atoms initially binding beneath the film from their Ru binding sites). While less drastic in terms of net peak shifts due to the increasing dominance of larger supported clusters at lower temperatures, the same general behavior was also observed for all other coverages probed as a function of temperature.

3.2. Electron bombardment effects on SiO_2 hydroxylation

Due to its fully saturated siloxane-terminated (Si-O-Si) structure the SiO_2 bilayer film is inherently hydrophobic, with very low propensity for spontaneous hydroxylation, as demonstrated by the results of previous work aimed at investigating the degree and nature of hydroxyl groups forming upon exposure to water vapor under various UHV conditions [17]. In that case, the only condition that resulted in detectable hydroxylation was exposure to water at low temperature (<150 K) and subsequent thermal desorption of the condensed ice layers. TPD results from such a sample, where multilayer equivalents of D_2O were dosed at 100 K and subsequently desorbed by heating to 200 K, are provided in the lower trace in Fig. 2.

Upon close inspection, three distinct features may be distinguished in this spectrum, with peaks at ~250 K, 450 K, and 900 K. The peak position of the lower-temperature features is consistent with those attributed to desorption of free water (250 K) and sub-monolayer physisorbed water (450 K) in different hydrogen bonding configurations over amorphous silica particles [28]. By contrast, our previous study of this film has shown that the higher temperature peak results from the recombinative desorption of water initially bound as

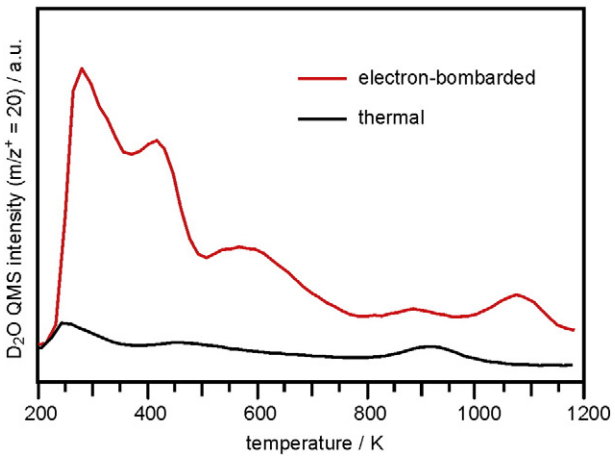

Fig. 2. TPD spectra are provided for SiO_2/Ru samples exposed to 5 L D_2O at 100 K and then either exposed (red trace) or not exposed (black trace) to a flux of high-energy electrons (50 μA; 200 V) for a duration of 60 s.

hydroxyls, most likely in the form of isolated silanols [17]. Given the relatively low concentration of water desorbing in this feature, consistent with at most ~1 [OH] per every 100 surface Si atoms, it has been suggested that such hydroxyls form exclusively at defect sites, with subsequent scanning tunneling microscopy (STM) studies conducted over monolayer $SiO_{2.5}$/Ru showing a preference for the junction nodes of three non-equivalent polygons within the silica framework [29].

As the defect concentration within bilayer SiO_2 films tends to be low and difficult to control without the addition of dopants or variation in the nature of the supporting metal substrate [30,31], alternative methods have been sought out to controllably manipulate hydroxylation in situ without permanently altering the sample, and electron bombardment of the ice-covered film has proven to provide a suitable means of accomplishing this. While a more detailed study aimed at better elucidating the mechanism by which this occurs is intended for subsequent publication [18], comparison of the upper and lower plots in Fig. 2, for which this procedure was and, respectively, was not employed, provides direct evidence of the effect.

The most obvious difference between the TPD taken from the electron-bombarded sample and its non-irradiated counterpart is the emergence of a new desorption feature at ~1070 K, which suggests the presence of a new hydroxyl species, most likely resulting from the breaking of siloxane bonds within the previously defect-free portions of the film. Interestingly, the size, shape, and position of the peak relating to recombination of defect-mediated hydroxyl groups, which is located at ~860 K in D_2O TPD from pristine SiO_2/Ru, remains roughly unchanged following electron bombardment, suggesting that this procedure does not significantly affect the formation of these species within our range of conditions. The increased energy needed to desorb the electron bombardment-induced hydroxyls at ~1070 K is indicative of isolated silanols with greater OH-OH separation relative to those forming thermally at defects [28].

At lower temperatures, we note peaks at 300 K and 450 K, albeit with much greater intensity than for the non-bombarded case. In addition, we now also clearly observe a high-energy desorption tail extending to temperatures beyond those expected for desorption of hydrogen-bonded water [28]. Some portion of the signal detected within this range of intermediate temperatures (~550–800 K) most likely results from desorption of (hydrogen-bonded) vicinal OH groups, the presence of which may also account for the formation of some of the isolated silanols subsequently desorbing at higher temperatures [28]. While quantitative disentanglement of the features relating to desorption of vicinal hydroxyls and hydrogen-bonded water is not readily achievable from our single spectrum, the largest changes to the D_2O TPD clearly relate to the desorption of additional physisorbed water molecules

following electron beam exposure. As electron bombardment clearly results in a significantly increased abundance of hydroxyl groups at the silica surface, the corresponding increase in the number of water molecules hydrogen-bonded to these moieties is not surprising, and to the extent that the amount of water desorbing in these features is more than twice the number desorbing from the higher temperature features, the number of water molecules binding per hydroxyl might exceed one.

3.3. Effect of water adsorption and electron bombardment on Pd permeability

To investigate the extent to which electron bombardment-induced hydroxylation processes affect the resultant porosity of bilayer SiO_2/Ru, we conducted a series of experiments using Pd adsorption to probe changes in these characteristics relative to 5 different sample preparation protocols, which consisted of (a) condensation of multilayer D_2O ice at 100 K, (b) electron bombardment of samples equivalent to those in (a) at 100 K, (c) thermal desorption of the electron-bombarded ice layer via heating samples consistent with (b) to 200 K (equivalent to the procedure employed to create the sample used to generate the upper plot in Fig. 2), (d) thermal desorption of the non-bombarded ice layer via heating samples consistent with (a) to 200 K (equivalent to the procedure employed to create the sample used to generate the lower plot in Fig. 2), and (e) preservation of the pristine, uncovered silica film (equivalent to the samples used to produce the temperature-dependent XPS plots in Fig. 1). As a means of indirectly tracking the variation in surface mobility relative to these preparation conditions, we collected Pd 3d XPS data from samples covered with 0.05, 0.20, 0.50, and 1.0 ML at temperatures ranging from 100 to 600 K in increasing increments of 100 K. For reference, representative data are again provided for the most sensitive dose (0.05 ML) following each of the five preparation conditions (a–e) at 100 and 200 K in Fig. 3.

Starting with the ice-covered sample at 100 K (Fig. 3a), we note the distinct absence of the feature previously noted at 335.1 eV for pristine SiO_2/Ru covered with the same concentration of Pd at this temperature (Fig. 3e). Given the sub-silica designation of the atoms resulting in this peak, its absence when dosing samples completely covered with multiple layers of ice is not surprising due to the physical barriers impeding the diffusion of Pd to, and then through, the silica film. The solitary broad peak centered at 338.0 eV is therefore indicative of binding and nucleation of a distribution of small Pd aggregates and atoms above the ice layer, where reduced final-state screening is expected to result in the observed increased BE relative to bulk reference samples, like Pd(111). After heating this sample to 200 K, and thereby removing the bulk of the physisorbed D_2O, we note a downward shift to 336.6 eV, which is more consistent with the peak position associated with Pd supported over pristine SiO_2/Ru in this temperature range (see Fig. 1). To the extent that we do not see significant growth of the lower BE feature, we may conclude that Pd nucleation and hydroxylation, sufficient to fully impede subsequent diffusion of metal atoms through the silicate, must occur prior to ice-layer desorption. Furthermore, the peak broadening noted when transitioning across this temperature range is most likely indicative of dehomogenization in some combination of the size and chemical-state distributions of the silica-bound Pd remaining on the surface following ice removal.

When electron bombarding the ice layer prior to Pd adsorption (Fig. 3b), we note several changes relative to the non-bombarded case. Most notably, we can no longer fit the XPS spectrum using a single 3d line shape, which indicates the binding of different types of Pd on this sample. Of the two largest features, one appears above (BE = 339.5 eV) and the other below (BE = 337.2 eV) the BE noted in the lower plot for D_2O-supported Pd (Fig. 3a). Based on qualitative agreement with previous results on other oxide supports [16], the appearance of the higher BE feature is tentatively assigned to the emergence of Pd in an oxidized chemical state via interaction with newly formed OH radicals [32], although D_2, O_2, and D_2O_2 are also expected to be generated within the ice layer during exposure to high-energy electrons (D_2 was readily observed in subsequent TPDs from such samples) [33]. The second peak shifting to slightly lower BE relative to the ice-bound case might simply reflect electron-stimulated desorption of the ice multilayers, such that the non-hydroxylated Pd ends up in a state closer to that of SiO_2- rather than D_2O-supported clusters. This notion is supported by the inclusion of a small peak at 335.1 eV, which suggests some degree of accessibility to the pores within the SiO_2 film, and time-dependent LEED experiments conducted at 200 eV over equivalent amorphous ice-covered samples, which gradually sharpen to reveal the underlying SiO_2/Ru pattern as a function of e^- exposure (i.e., suggestive of ice-layer desorption). Regardless of the exact nature of the various Pd species giving rise to the primary features, what is

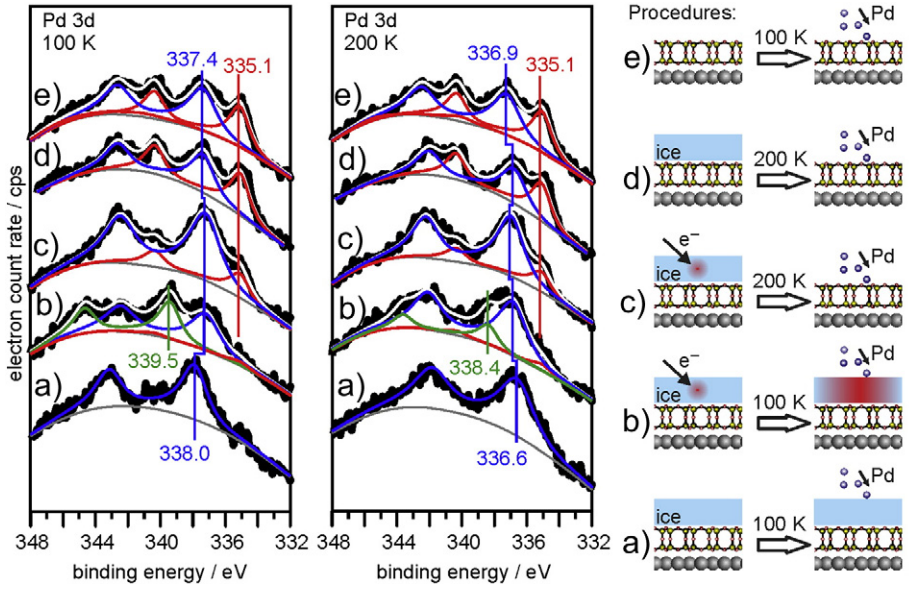

Fig. 3. Pd 3d XP spectra are provided at 100 K (left) and 200 K (middle) for five different sample preparation conditions (schematically shown on the right). The specific conditions employed following SiO_2/Ru growth and characterization were (a) exposure to 5 L D_2O at 100 K and subsequent deposition of Pd at the same temperature; (b) exposure to 5 L D_2O at 100 K, electron bombardment, and subsequent deposition of Pd at the same temperature; (c) exposure to 5 L D_2O at 100 K, electron bombardment at the same temperature, and subsequent UHV annealing to 200 K prior to deposition of Pd at 100 K; (d) exposure to 5 L D_2O at 100 K, and subsequent UHV annealing to 200 K prior to deposition of Pd at 100 K; and (e) deposition of Pd directly over the pristine film.

clear is that nearly all of the Pd is again blocked from penetrating the pores within the silica film when dosed over this sample. While we do note some degree of additional pore penetration when heating this sample to 200 K, as evidenced by growth of the peak component at 335.1 eV, most of the Pd again remains bound in some manner to the silica film following full multilayer D_2O thermal desorption. Based on the growth of the 337.3 eV feature at the expense of the higher BE peak (at 339.5 eV in the 100 K spectrum), we conclude that much of the initially oxidized Pd is reduced via some combination of dehydration, dehydroxylation, and further particle nucleation within this temperature range.

Since the extent to which incomplete electron-stimulated desorption may leave behind residual, Pd-SiO_2 interaction blocking, multilayer ice barriers cannot be directly ascertained in the previous case (Fig. 3b), samples prepared in the next experiment (Fig. 3c) were created in the same manner but first heated to 200 K to fully desorb the ice multilayers before loading Pd. Indeed, fully removing the amorphous ice blocking layer results in greater access to the pores within the film, as reflected by the presence of a well-defined low BE peak attributed to Ru-bound atoms at 335.1 eV. Nonetheless, the peak ratio between the higher and lower BE features, which greatly favors the former, tells us that interactions with oxide-bound water and hydroxyl groups do significantly increase the likelihood of metal nucleation and binding over the silica film relative to equivalent samples created by depositing Pd on the pristine film (Fig. 3e).

Unlike the previous examples, heating this sample to 200 K results in virtually no changes to the XPS, which further substantiates the idea that the effects noted in the other cases are directly correlated to changes in the nature of Pd atoms initially bound over multilayers of ice as those layers disappear from the surface (i.e., decreased chemical interaction with various species present within the ice layer and further diffusion and nucleation into new binding arrangements over the oxide film). Perhaps not surprisingly, when conducting the same experiment in the absence of the electron bombardment step (Fig. 3d), which results in comparatively negligible concentrations of hydroxyls and surface-bound water (see Fig. 2), we note very little difference relative to XPS spectra obtained after depositing equivalent doses of Pd over pristine samples (Fig. 3e). Furthermore, we again note little change in XPS between 100 and 200 K, further indicating that, once formed, Ru- and silica-bound Pd species remain stable within this range of temperatures, independent of the sub-monolayer pre-adsorbed hydroxyl and molecular water concentrations.

In terms of permeability, the results in Fig. 3 can be broken down into three distinct groups based on the relative abundance of atoms binding at Ru sites as a function of preparation condition. To help visualize differences between these groups, the relative contribution of the Ru-bound peak (335.1 eV) to the overall Pd 3d XPS spectrum has been plotted vs. temperature (from 100 to 600 K) in Fig. 4 for each of the conditions previously discussed. As already pointed out, the various preparation conditions result in three distinctly different surface characteristics at low temperature, which may be described as porous (d and e), semi-porous (c), and non-porous (a and b). Interestingly, while the hydroxylated film (c) results in a greater propensity for silica-localized binding and nucleation upon low-temperature adsorption, the subsequent thermally induced modifications show the same qualitative trends in every case (i.e., consistent with the trends in Fig. 1), such that surface diffusion processes result in the gradual growth of larger supported clusters above 300 K and an eventual convalescence with sub-surface Pd at temperatures exceeding 500 K.

In an attempt to disentangle the roles played by the various hydroxyl groups and the hydrogen-bonded water molecules associated with them, an additional set of experiments were conducted with pre-hydroxylated samples heated to different temperatures prior to Pd adsorption (Fig. 5). As expected, heating below 300 K, which is below the desorption threshold for silica-bound molecular water, has no effect on the permeability of the samples (Fig. 5a). By contrast, pre-annealing

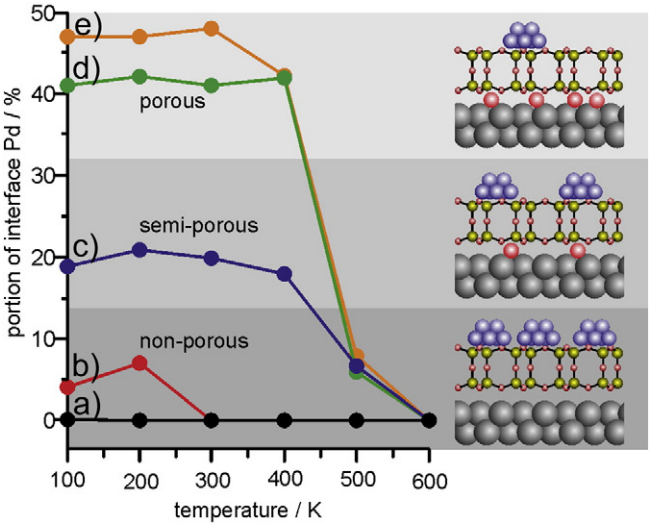

Fig. 4. Left: The annealing temperature dependence of the portion of Pd confined at the Ru interface (the relative intensity of the XPS feature at 335.1 eV) is plotted for each of the five conditions (a–e) described in Fig. 3. The schematic on the right illustrates the Pd binding characteristics found for the different conditions, which result in non-porous (a, b), semi-porous (c) and porous (d, e) states of the silica film with respect to Pd diffusion.

temperatures from 300 to 650 K (Fig. 5b and c), which span a range covering the full desorption of physisorbed water molecules and partial removal of vicinal hydroxyls, do affect this characteristic, such that the samples become steadily more permeable with increasing temperature. In fact, samples prepared by annealing previously electron-bombarded ice-covered samples to 650 K (Fig. 5c) result in Pd adsorption behavior that is essentially indistinguishable from the porous films (Fig. 3d and e). While any potential role of vicinal hydroxyl groups is difficult to surmise, the results of this work show a clear dependence on the concentration of hydroxyl-bound molecular water, even before the expected onset for vicinal OD recombination, and from that correlation, we conclude that the molecular D_2O species are predominantly responsible for limiting Pd diffusion through the film; most likely via simple pore blockage. This result is in stark contrast with those obtained for Pd adsorption over MgO thin films [16], where strong Pd-OD anchoring interactions greatly influenced the subsequent thermal diffusion and nucleation of Pd initially deposited on hydroxylated vs. non-hydroxylated supports. On MgO, the interaction of Pd and OD is of a redox-type, leading to Pd oxidation and D_2 evolution [16]. Although

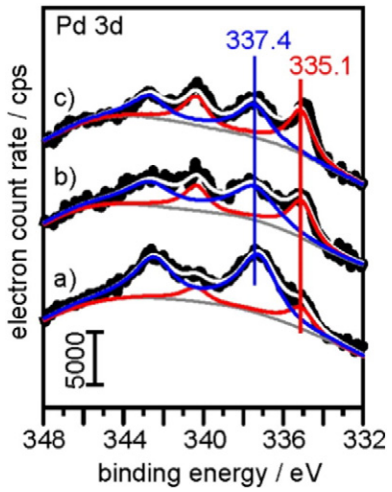

Fig. 5. Pd 3d XP spectra of 0.05 ML Pd deposited on hydroxylated SiO_2/Ru, which has been prepared by adsorption of 5 L D_2O at 100 K, followed by electron bombardment and subsequent annealing to a) 200 K, b) 300 K, and c) 650 K.

D_2 desorption has been observed from the Pd-loaded hydroxylated silica samples as well, in this case the source of D_2 are D atoms created during the electron bombardment step in the D_2O ice layer, which diffuse out of the ice layer to the silica surface and Ru-silica interface and get trapped on Pd particles upon subsequent Pd deposition (see *Supporting Information*).

3.4. Comparisons with solution-based Pd deposition via $[Pd(NH_3)_4]^{2+}$ adsorption

Highly dispersed Pd particles find widespread use in a number of silica-supported reaction systems [19–24,34–43], with many of those prepared via impregnation of silicas with Pd salts (chloride, nitrate) or adsorption of Pd complexes (acetate, ammine). For the latter, several studies have been conducted to characterize the adsorption, decomposition, nucleation, and activation of ligand-coordinated Pd precursor species brought into contact with high surface-area silicas within aqueous environments [21,22,24]. While an ion-exchange mechanism has previously been suggested to dominate the interaction of ammine-complexes with the silica support, more recent work favors an interpretation based upon strong electrostatic adsorption [24].

For this work, we have employed exposure to 1000 ppm $[Pd(NH_3)_4]Cl_2$ within pH 12 NaOH aqueous solution for a period of 1 h to attain comparative results from our model bilayer SiO_2/Ru(0001) support. The selected alkalinity falls on the higher end of the range commonly used within more applied settings and was chosen to provide large enough $[OH^-]$ concentration to generate significant quantities of silanol sites, which are needed to facilitate adsorption of the dissolved $[Pd(NH_3)_4]^{2+}$ moieties, without resulting in significant dissolution-induced film degradation [44]. That being said, the goal of this work was not the optimization of the adsorption process to best suit our model support but instead to use the well-defined nature of our simplified material to provide a platform to better characterize the Pd deposition, nucleation, and particle formation dynamics in a manner capturing the full range of overall complexities expected to coexist during the generation of more applied materials under similar conditions.

To track the condition-dependent evolution of Pd remaining on the surface following our solution-based deposition, we have generated Fig. 6, which shows the Pd 3d (Fig. 6a) and N 1s (Fig. 6b) XPS regions along with their comparative peak intensities (Fig. 6c) throughout a sequence of treatments typical during precursor transformation and activation processes employed when generating applied analogs of our model catalyst system. Starting with the sample immediately following exposure to the aqueous precursor solution (i), we note clear signals indicative of both N and two types of Pd at respective BEs of 400.6, 339.0, and 337. 5 eV, which provides clear evidence of interaction between the aqueous precursor and the SiO_2/Ru model support. While detailed direct interpretation of the peak locations in the absence of significant supporting information is dubious due to undetermined charging and final-state contributions, all Pd and N species appear to initially adsorb within cationic chemical-state configurations based on first-order approximations arising from simplified initial-state comparisons with literature data [45]. Such a finding is qualitatively consistent with results from previous investigations of the interaction of $[Pd(NH_3)_4]^{2+}$ with silica gels, which suggest Pd^{2+} configurations following liquid exposure [21–23]. While $[Pd(NH_3)_4]^{2+}$ groups are expected to adsorb as fully intact coordination spheres at pHs above 10.5 [21,22], the presence of two distinct Pd XPS features may suggest some degree of ligand liberation or substitution during the brief drying period prior to insertion within the sample transfer and UHV chambers. Supporting this assertion, washing the samples with several mL of pH neutral ultrapure water, which is known to result in H_2O-NH_3 ligand exchange in tandem with Pd complex re-dissolution [21], leads to partial loss of both Pd 3d and N 1s XPS signals (i.e., precursor complex dissolution) and Pd peak shifts to lower BEs, which we tentatively assign to increasing H_2O:NH_3 ligand ratios surrounding the bound Pd^{2+} centers (Fig. 6, (ii)). Consistent with

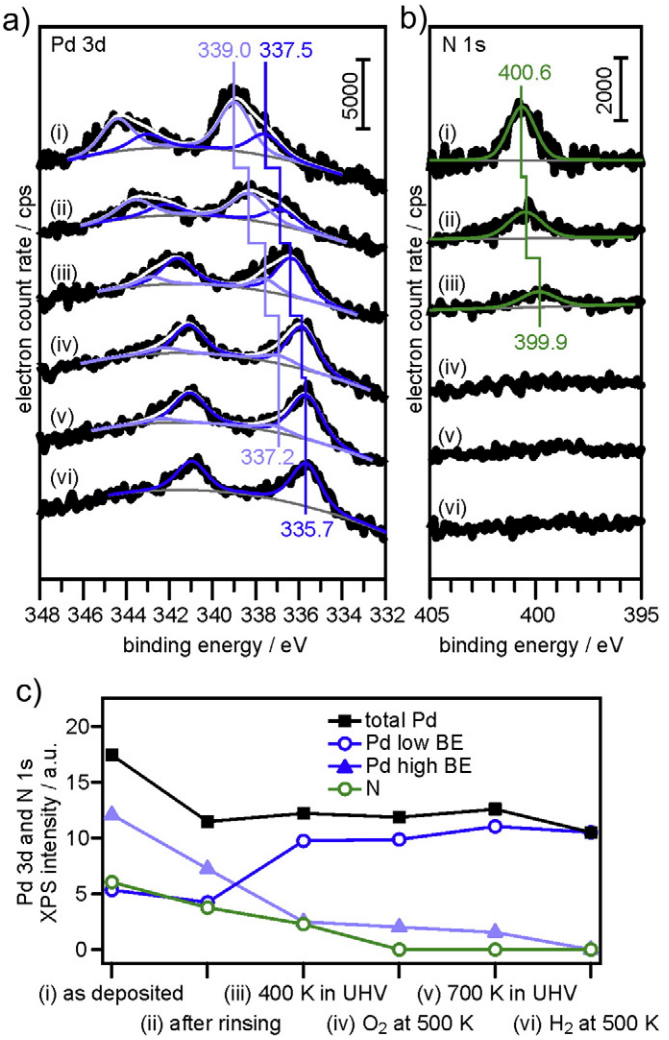

Fig. 6. Pd 3d (a) and N 1s (b) XP spectra are provided as a function of condition following SiO_2/Ru exposure to 1000 ppm $[Pd(NH_3)_4]Cl_2$ pH 12 NaOH precursor solution for 1 h at room temperature. Comparison of the higher BE, lower BE, and total Pd 3d peak intensities relative to that collected for N 1s as a function of post-deposition sample treatment.

this hypothesis, similar BE trends are noted within the literature when comparing various NH_3-bound and O-bound Pd^{2+} centers [46]. Notably, we see no evidence of Pd film penetration, which we ascribe to the presence of the large ligand spheres surrounding the Pd centers that are also noted to result in high dispersion over higher surface-area silicates [19–23,34–38].

After heating the washed samples to 400 K within UHV, we note continued shifts of both Pd 3d features to lower BE (Fig. 6, (iii)). Concomitant with these shifts, we also note a significant growth of the lower BE peak at the expense of the higher BE component. Following the peak assignments described above, this trend suggests a continued loss of NH_3 ligands from the Pd^{2+} centers, which coincides with N 1s peak attenuations also noted following this treatment. Notably, the N 1s peak intensity falls to roughly half that noted immediately following deposition following this treatment, which is consistent with previous findings suggesting the presence of $[(SiO)_2]^{2-}[Pd(NH_3)_2]^{2+}$ adsorption configurations following drying-induced precursor decomposition in similar environments [22]. While the slightly increased total Pd 3d signal intensity likely reflects decreased ligand-related attenuation resulting from (NH_3) liberation, loss of carbonaceous species are also likely to play some role since C 1s signal (not shown) also shows significant reduction following this step. Note that while adventitious carbon contamination was unavoidable following liquid-UHV sample

exchange, no other extraneous peak contributions (i.e., Na, Cl, etc.) could be detected following liquid exposure.

To deal with unavoidable carbon species, which often poison interfacial active sites, most realistic catalyst preparations include an oxidation step to fully remove all remaining hydrocarbons via chemical combustion. In our case, this was done via exposure to 1000 L O_2 at 500 K (Fig. 6, (iv)), which does result in complete loss of the C 1s peak contribution to the XPS spectrum. In addition, visual inspection of Fig. 6 shows complete removal of N species following this step, which is again consistent with previous studies that suggest the formation of a combination of $[(SiO)_2]^{2-}Pd^{2+}$ and Pd^0/SiO_2 following similar treatment. Based on the Pd 3d peak coalescence/sharpening and BE reduction following exposure to high temperature reducing conditions, such as heating to 700 K in UHV (Fig. 6, (v)) and dosing 1000 L H_2 at 500 K (Fig. 6, (vi)), we conclude that such treatment results in the conversion of any remaining $Pd^{\delta+}$ to Pd^0 and some degree of Pd cluster growth via diffusion and nucleation processes, which is also consistent with findings from more applied catalysis analogs under similar preparation conditions [22].

Comparing the 3d XPS spectrum following the full sequence of treatments for the wet-chemically deposited Pd (Fig. 6) to those observed for various coverages of vacuum-deposited Pd (Fig. 1) at different temperatures, we note total peak intensities consistent with ~2% ML at a slightly higher final BE (335.7 eV). While subtle variations to Pd sensitivity and chemical state due to variations in relative particle structures and the influence of undetectable quantities of coadsorbed species cannot be absolutely ruled out as potential contributing factors, we conclude that the small differences between these spectra instead reflect the presence of a lower coverage of more dispersed Pd^0 particles following the liquid-based metal loading methodology. Consistent with this conclusion, we note nearly constant Pd sensitivity over a wide range of loadings (0.05–1.00 ML) in Fig. 1b, indicating limited influence from structure-based attenuation effects, and CO TPD behavior (not shown) that is both qualitatively and quantitatively similar with the lowest coverage Pd/SiO_2 sample created within UHV following the 600 K annealing step (Fig. 1a), suggesting the presence of chemically similar Pd nanoparticles with similar, but possibly somewhat higher, surface area-to-volume ratios (i.e., more dispersed).

4. Conclusion

In this work, we have demonstrated a means of readily controlling the surface termination of bilayer SiO_2/Ru by varying the concentration of surface hydroxyls with an electron bombardment-mediated approach. Films created with larger hydroxyl concentrations also contained more hydrogen-bonded water (desorbing near room temperature), which resulted in decreased probabilities of Pd diffusion through the porous silica network at low temperatures. When heated to temperatures exceeding the threshold for molecular water desorption before dosing Pd, such effects were no longer noted, indicating that the more strongly bound hydroxyls likely play little role in influencing Pd diffusion or film permeability in the absence of these additional water species, which is in stark contrast to previous studies over other oxides, where hydroxyl groups have been shown to act as anchoring sites for Pd adsorption and nucleation [16]. Instead, the lower-temperature effects noted within this work more likely derive from physical constriction of the size and number of pores within the film by the presence of hydrogen-bonded water molecules. Independent of initial silica hydroxylation and Pd binding configuration distributions, all Pd/SiO_2/Ru samples created within UHV coalesce into predominantly silica-supported clusters of increasing size with increasing loadings and sample temperatures. When bringing Pd to the SiO_2/Ru interface via adsorption of $[Pd(NH_3)_4]^{2+}$ ions from aqueous (pH 12) solution, notably different adsorption behavior is observed, whereby large precursor complexes precluded Pd permeation through the film and subsequently experienced cumulative silicate-confined decomposition and nucleation under increasingly aggressive environmental conditions and elevated temperatures within UHV. Similarities in XPS and CO TPD between samples created exclusively within UHV and via wet-chemical exposure to Pd precursor species establish the viability of this system for subsequent comparative studies under a wider range of conditions to explore the potential influences of a number of various additional aqueous parameters as a means of better informing more rational designs of future applied catalyst recipes.

Acknowledgment

W.E.K. is grateful to the Alexander von Humboldt foundation for providing a fellowship. M.S. and S.P. acknowledge support by the European Union through ERC grant agreement No. 280070 (STRUBOLI). H.J.F. acknowledges financial support by the German-Israeli Foundation (No.1236). This work was supported by the German Research Foundation through Collaborative Research Center grant CRC1109.

Appendix A. Supplementary data

Supplementary data to this article can be found online at http://dx.doi.org/10.1016/j.susc.2015.12.030.

References

[1] L. Giordano, G. Pacchioni, Oxide films at the nanoscale: new structures, new functions, and new materials, Acc. Chem. Res. 44 (2011) 1244.
[2] T. Schröder, M. Adelt, B. Richter, M. Naschitzki, M. Bäumer, H.-J. Freund, Epitaxial growth of SiO_2 on Mo(112), Surf. Rev. Lett. 7 (2000) 7.
[3] Z. Zhang, Z.Q. Jiang, Y.X. Yao, D.L. Tan, Q. Fu, X.H. Bao, Preparation and characterization of atomically flat and ordered silica films on a Pd(100) surface, Thin Solid Films 516 (2008) 3741.
[4] M. Kundu, Y. Murata, Growth of single-crystal SiO_2 film on Ni(111) surface, Appl. Phys. Lett. 80 (2002) 1921.
[5] T. Tanemura, S. Sato, M. Kundu, C. Yamada, Y. Murata, Growth of single-crystal SiO_2 clusters on Si(001) surface, J. Appl. Phys. 105 (2009) 074310.
[6] D. Löffler, J.J. Uhlrich, M. Baron, B. Yang, X. Yu, L. Lichtenstein, L. Heinke, C. Büchner, M. Heyde, S. Shaikhutdinov, H.-J. Freund, R. Wlodarczyk, M. Sierka, J. Sauer, Growth and structure of crystalline silica sheet on Ru(0001), Phys. Rev. Lett. 105 (2010) 146104.
[7] S. Shaikhutdinov, H.-J. Freund, Ultrathin silica films on metals: the long and winding road to understanding the atomic structure, Adv. Mater. 25 (2013) 49.
[8] C. Büchner, L. Lichtenstein, X. Yu, J.A. Boscoboinik, B. Yang, W.E. Kaden, M. Heyde, S. Shaikhutdinov, R. Wlodarczyk, M. Sierka, J. Sauer, H.-J. Freund, Ultrathin silica films: the atomic structure of two-dimensional crystals and glasses, Chem. Eur. J. 20 (2014) 9176.
[9] L. Lichtenstein, C. Büchner, B. Yang, S. Shaikhutdinov, M. Heyde, M. Sierka, R. Wlodarczyk, J. Sauer, H.-J. Freund, The atomic structure of a metal-supported vitreous thin silica film, Angew. Chem. Int. Ed. 51 (2012) 404.
[10] L. Lichtenstein, M. Heyde, H.-J. Freund, Crystalline-vitreous interface in two dimensional silica, Phys. Rev. Lett. 109 (2012) 106101.
[11] B. Yang, W.E. Kaden, X. Yu, J.A. Boscoboinik, Y. Martynova, L. Lichtenstein, M. Heyde, M. Sterrer, R. Wlodarczyk, M. Sierka, J. Sauer, S. Shaikhutdinov, H.-J. Freund, Thin silica films on Ru(0001): monolayer, bilayer and three-dimensional networks of SiO_4 tetrahedra, PCCP 14 (2012) 11344.
[12] E. Emmez, B. Yang, S. Shaikhutdinov, H.-J. Freund, Permeation of a single-layer SiO_2 membrane and chemistry in confined space, J. Phys. Chem. C 118 (2014) 29034.
[13] C. Büchner, L. Lichtenstein, S. Stuckenholz, M. Heyde, F. Ringleb, M. Sterrer, W.E. Kaden, L. Giordano, G. Pacchioni, H.-J. Freund, Adsorption of Au and Pd on ruthenium-supported bilayer silica, J. Phys. Chem. C 118 (2014) 20959.
[14] L. Giordano, A. Del Vitto, G. Pacchioni, Au and Pd atoms adsorbed on pure and Ti-doped SiO_2/Mo(112) films, J. Chem. Phys. 124 (2006) 034701.
[15] M.A. Brown, Y. Fujimori, F. Ringleb, X. Shao, F. Stavale, N. Nilius, M. Sterrer, H.-J. Freund, Oxidation of Au by surface OH: nucleation and electronic structure of gold on hydroxylated MgO(001), J. Am. Chem. Soc. 133 (2011) 10668.
[16] Y. Fujimori, W.E. Kaden, M.A. Brown, B.R. Cuenya, M. Sterrer, H.-J. Freund, Hydrogen evolution from metal-surface hydroxyl interaction, J. Phys. Chem. C 118 (2014) 17717.
[17] B. Yang, E. Emmez, W.E. Kaden, X. Yu, J.A. Boscoboinik, M. Sterrer, S. Shaikhutdinov, H.-J. Freund, Hydroxylation of metal-supported sheet-like silica films, J. Phys. Chem. C 117 (2013) 8336.
[18] X. Yu, E. Emmez, Q. Pan, B. Yang, S. Pomp, W.E. Kaden, M. Sterrer, S. Shaikhutdinov, H.-J. Freund, I. Goikoetxea, R. Wlodarczyk, J. Sauer, Electron stimulated hydroxylation of a metal supported silicate film, PCCP, accepted. http://dx.doi.org/10.1039/C5CP06852E.
[19] J.S. Rieck, A.T. Bell, The influence of dispersion on the interactions of H_2 and CO with Pd/SiO_2, J. Catal. 103 (1987) 46.
[20] S. Ichikawa, H. Poppa, M. Boudart, Disproportionation of CO on small particles of silica-supported palladium, J. Catal. 91 (1985) 1.

[21] A.L. Bonivardi, M.A. Baltanas, Preparation of Pd/SiO_2 catalysts for methanol synthesis. 1. Ion-exchange of $Pd(NH_3)_4(ACO)_2$, J. Catal. 125 (1990) 243.
[22] A.L. Bonivardi, M.A. Baltanas, Preparation of Pd/SiO2 catalysts for methanol synthesis. 2. Thermal decomposition of $Pd(NH_3)_4^{2+}$ SiO_2, Thermochim. Acta 191 (1991) 63.
[23] B. Pommier, P. Gelin, On the nature of Pd species formed upon exchange of H-ZSM5 with $Pd(NH_3)_4^{2+}$ and calcination in O_2, PCCP 1 (1999) 1665.
[24] L. Jiao, J.R. Regalbuto, The synthesis of highly dispersed noble and base metals on silica via strong electrostatic adsorption: I. Amorphous silica, J. Catal. 260 (2008) 329.
[25] W.E. Kaden, C. Büchner, L. Lichtenstein, S. Stuckenholz, F. Ringleb, M. Heyde, M. Sterrer, H.-J. Freund, L. Giordano, G. Pacchioni, C.J. Nelin, P.S. Bagus, Understanding surface core-level shifts using the auger parameter: a study of Pd atoms adsorbed on ultrathin SiO_2 films, Phys. Rev. B 89 (2014) 115436.
[26] P.S. Bagus, A. Wieckowski, H.-J. Freund, The contribution of lattice strain to core-level binding energy shifts in metal nanoparticles: generality and origin of the shifts, Comput. Theor. Chem. 987 (2012) 22.
[27] G.K. Wertheim, S.B. Dicenzo, S.E. Youngquist, Unit charge on supported gold clusters in photoemission final-state, Phys. Rev. Lett. 51 (1983) 2310.
[28] L.T. Zhuravlev, The surface chemistry of amorphous silica. Zhuravlev model, Colloids Surf., A 173 (2000) 1.
[29] B. Yang, S. Shaikhutdinov, H.-J. Freund, Tuning spatial distribution of surface hydroxyls on a metal-supported single-layer silica, J. Phys. Chem. Lett. 5 (2014) 1701.
[30] J.A. Boscoboinik, X. Yu, B. Yang, S. Shaikhutdinov, H.-J. Freund, Building blocks of zeolites on an aluminosilicate ultra-thin film, Microporous Mesoporous Mater. 165 (2013) 158.
[31] X. Yu, B. Yang, J.A. Boscoboinik, S. Shaikhutdinov, H.-J. Freund, Support effects on the atomic structure of ultrathin silica films on metals, Appl. Phys. Lett. 100 (2012) 151608.
[32] N.G. Petrik, R.J. Monckton, S.P.K. Koehler, G.A. Kimmel, Distance-dependent radiation chemistry: oxidation versus hydrogenation of CO in electron-irradiated H_2O/CO/H_2O ices, J. Phys. Chem. C 118 (2014) 27483.
[33] W.J. Zheng, D. Jewitt, R.I. Kaiser, Electron irradiation of crystalline and amorphous D_2O ice, Chem. Phys. Lett. 435 (2007) 289.
[34] M.L. Toebes, J.A. van Dillen, Y.P. de Jong, Synthesis of supported palladium catalysts, J. Mol. Catal. A Chem. 173 (2001) 75.
[35] H. Deligianni, R.L. Mieville, J.B. Peri, State of Pd in active methanol synthesis catalysts, J. Catal. 95 (1985) 465.
[36] T.C. Chang, J.J. Chen, C.T. Yeh, Temperature-programmed reduction and temperature-resolved sorption studies of strong metal support interaction in supported palladium catalysts, J. Catal. 96 (1985) 51.
[37] F. Fajula, R.G. Anthony, J.H. Lunsford, Methane and methanol synthesis over supported palladium catalysts, J. Catal. 73 (1982) 237.
[38] Y. Kikuzono, S. Kagami, S. Naito, T. Onishi, K. Tamaru, Selective hydrogenation of carbon monoxide on palladium catalysts, Faraday Discuss. 72 (1981) 135.
[39] A.M. Kazi, B. Chen, J.G. Goodwin, G. Marcelin, N. Rodriguez, T.K. Baker, Li^+ promotion of Pd/SiO_2: the effect on hydrogenation, hydrogenolysis, and methanol synthesis, J. Catal. 157 (1995) 1.
[40] M. Viniegra, G. Córdoba, R. Gómez, Gas phase hydrogenation of o-xylene over palladium catalysts, J. Mol. Catal. 58 (1990) 107.
[41] S. Naito, M. Iwahashi, I. Kawakami, T. Miyao, Marked particle size and support effect of Pd catalysts upon the direct decomposition of nitric oxide, Catal. Today 73 (2002) 355.
[42] B. Nohair, C. Especel, G. Lafaye, P. Marécot, L.C. Hoang, J. Barbier, Palladium supported catalysts for the selective hydrogenation of sunflower oil, J. Mol. Catal. A Chem. 229 (2005) 117.
[43] N.S. Figoli, P.C. Largentiere, A. Arcoya, X.L. Seoane, Modification of the properties and sulfur resistance of a Pd/SiO_2 catalyst by La addition, J. Catal. 155 (1995) 95.
[44] W.E. Kaden, S. Pomp, M. Sterrer, H.J. Freund, to be published.
[45] J.F. Moulder, W.F. Stickle, P.E. Sobol, K.D. Bomben, Handbook of X-ray Photoelectron Spectroscopy: A Reference Book of Standard Spectra for Identification and Interpretation of XPS Data, Physical Electronics, 1995.
[46] A.V. Naumkin, A. Kraut-Vass, S.W. Gaarenstroom, C.J. Powell, NIST X-ray Photoelectron Spectroscopy Database, 2012 (srdata.nist.gov/xps/).